Electrochimica Acta 56 (2011) 5898–5903

Contents lists available at ScienceDirect

Electrochimica Acta

journal homepage: www.elsevier.com/locate/electacta

Ni–W coatings electrodeposited on carbon steel: Chemical composition, mechanical properties and corrosion resistance

M.P. Quiroga Argañaraz[a], S.B. Ribotta[a], M.E. Folquer[a,*], L.M. Gassa[b], G. Benítez[b], M.E. Vela[b,1], R.C. Salvarezza[b,1]

[a] INQUINOA-CONICET, Instituto de Química Física, Facultad de Bioquímica, Química y Farmacia, Universidad Nacional de Tucumán, Ayacucho 471, (4000) San Miguel de Tucumán, Argentina
[b] Instituto de Investigaciones Fisicoquímicas Teóricas y Aplicadas (INIFTA), Universidad Nacional de La Plata-CONICET, Suc. 4, C.C. 16, (1900) La Plata, Argentina

ARTICLE INFO

Article history:
Received 3 January 2011
Received in revised form 29 April 2011
Accepted 30 April 2011
Available online 7 May 2011

Keywords:
Pulse electrodeposition
Ni–W coatings
AFM
XPS
Corrosion resistance

ABSTRACT

Hard, ductile and adherent nanostructured Ni–W coatings were electrodeposited on carbon steel from electrolyte solutions containing sodium tungstate, nickel sulfate and sodium citrate, using different current pulse programs. Current pulse frequency was the dominant factor to define chemical composition, grain size, thickness and hardness. According to the electrodeposition conditions the deposited coatings showed 15–30 at% W, the grain size ranged from 65 to 140 nm, and the hardness varied from 650 to 850 Hv. Tungsten carbide also present in the coating contributed to its hardness. The corrosion resistance of the Ni–W coated steel was tested by potentiodynamic polarization in a neutral medium containing sulphate ions. The Ni–W coating protected the carbon steel from localized corrosion induced by sulphate anions.

1. Introduction

In these last years the interest in electrodeposited tungsten (W) alloys with iron group metals has increased due to their excellent properties and engineering applications. These alloys can only be obtained through an induced codeposition [1], that is, W is codeposited from aqueous solutions with an iron group metal forming an alloy [1–34]. In this respect, different reaction models were proposed to explain the codeposition mechanism, depending on which metal has been deposited with W and what the deposition conditions were [1,13–15,18,22,27,29]. Efforts to get plated nickel–tungsten (Ni–W) alloys were increased as they proved to have optimum hardness and good corrosion resistance. These improved characteristics, together with good ductility and high thermal stability, can be achieved when obtaining micro to nanostructured electrodeposits [15,17,28,30,34]. Besides, these plated alloys could be particularly suitable to protect steel pieces from corrosion and erosion in the oil and naval industries if they have the desired mechanical properties and good substrate adhesiveness. Solution composition (as well as concentration of the electrolyte), pH, temperature and current density are crucial to attain these goals. Ni–W deposits with similar composition can exhibit different structure and surface morphology [8,13,15–17,27,31,33]. In this sense, the different experimental procedures and even the substrate preparation can influence the results achieved. However, it would generally seem that as W content in the alloy increases, grain size diminishes [10,17,28,30,31,33,34].

In a large number of works the electroplating of nanocrystalline Ni–W deposits was carried out using direct current density [11,14–16,18,22,28,31,33]. However, pulse plating is an effective means of controlling the microstructure and composition of electrodeposits because it can be used to improve current distribution and modify mass transport [11,23]. Thus, different problems like hydrogen evolution and uneven deposits caused by mass transport may be overcome and pH local changes minimized. Several studies on pulse plated Ni [32,36], Ni–Mo [3,20], Co–W [4,21] and in the last years Ni–W alloys [29,30,34], are reported in the literature.

From the point of view of the practical interest that Ni–W alloys offer, it is fundamental to know their corrosion resistance. Hence, some authors carried out studies in NaCl and H_2SO_4 solutions that showed that the corrosion behaviour of these alloys is very complex, depending not only on W content, alloy structure and corrosion medium, but also on the component from the iron group metals and even on preparation conditions [9,16,24,31,33]. Thus, a general rule that defines their behavior cannot be established. Furthermore, there are no studies in neutral Na_2SO_4 solutions. They

* Corresponding author. Tel.: +54 381 4248170/4107218; fax: +54 381 4248169.
E-mail address: mefolquer@fbqf.unt.edu.ar (M.E. Folquer).
[1] ISE Member.

0013-4686/$ – see front matter © 2011 Elsevier Ltd. All rights reserved.
doi:10.1016/j.electacta.2011.04.119

are crucial when steel pieces have to be protected from corrosion, since the sulphate ion becomes more aggressive than the chloride ion in neutral and alkaline solutions, provoking pitting [37].

In this work, hard, ductile and adherent nanocrystalline Ni–W coatings were electrodeposited on carbon steel by different pulsating current programs. By using a multitechnique characterization approach we demonstrate that current pulse frequency was the dominant factor to define chemical composition, grain size, hardness and corrosion resistance of the electrodeposited Ni–W coating.

2. Experimental

Nanocrystalline Ni–W coatings were deposited on carbon steel (SAE 1020) sheets (area = 1 cm^2), which were previously polished with grit paper in decreasing size from 80 to 2500 followed by 0.3 μm alumina powder. Finally, they were rinsed with twice-distilled water.

The electrodeposited coatings were obtained galvanostatically by pulse electroplating using a Zahner IM6e potentiostat/galvanostat. The pulse scheme consisted in "on" time (τ_{on}) during which a reduction current of 70 mA cm^{-2} was applied and an "off" time (τ_{off}) during which a zero current was applied, where $\tau = \tau_{on} = \tau_{off}$ with $10 \leq \tau \leq 300$ s. The deposition time (t_{dep}) varied from 20 to 180 min.

The plating bath contained 0.06 M $NiSO_4{\cdot}6H_2O$, 0.14 M $Na_2WO_4{\cdot}2H_2O$, 0.5 M $Na_3C_6H_5O_7{\cdot}2H_2O$, 0.5 M NH_4Cl and 0.15 M NaBr (pH 9.5). In some experiments pH was adjusted to 7.0 using 25% citric acid solution. A fresh plating bath was prepared for each experiment using pure chemical reagents and twice-distilled water. During the plating the solution was gently stirred with a magnetic stirrer at 65 °C.

The metallic deposit surface morphology and bulk chemical composition were analyzed using a JEOL (JSM 6480 LV) scanning electron microscope (SEM) with an energy dispersive spectroscopy (EDS) detector, Thermo Electron, model NORAM System SIX NSS-100. The surface composition was evaluated by X-ray photoelectron spectroscopy (XPS) using a Mg Kα source (1253.6 eV) XR50, Specs GmbH and a hemispherical electron energy analyzer PHOIBOS 100, Specs GmbH.

Deposit roughness, surface morphology and crystal size were estimated in air in the contact mode with a Contact AFM commanded by a Nanoscope IIIa control unit from Veeco Instruments (Santa Barbara, CA, USA). Triangular silicon nitride probes (k = 0.58 N/m) from Veeco Instruments (Santa Barbara, CA, USA) were used in all measurements.

Microhardness measurements were carried out with a Shimadzu Microindenter with a Vickers indenter. Hardness measurements were performed on sample cross-sections applying a load of 15 g for 15 s. The thickness of coatings were determined from metallographic cross sections.

To evaluate corrosion resistance of the electrodeposited coatings, a single triangular potential sweep (STPS) between preset cathodic ($E_{s,c}$) and anodic ($E_{s,a}$) switching potentials, at potential scan rate (ν) in the $0.002\ V\ s^{-1} \leq \nu \leq 0.200\ V\ s^{-1}$ range was applied to the electrodeposited Ni–W coatings in a still phosphate-borate buffer (0.1 M KH_2PO_4 + 0.05 M $Na_2B_4O_7$) pH 8.00, with the addition of 1 M Na_2SO_4. In order to compare behaviours, similar experiments were carried out in the same solution with carbon steel (substrate), pure Ni and pure W electrodes at $\nu = 0.002\ V\ s^{-1}$. A standard three-electrode cell was used. A large area Pt sheet counter electrode and a saturated calomel reference electrode (SCE) were used. All potentials in the text were referred to the SCE (0.241 V vs SHE).

Experiments were made under purified N_2 gas saturation at 25 °C.

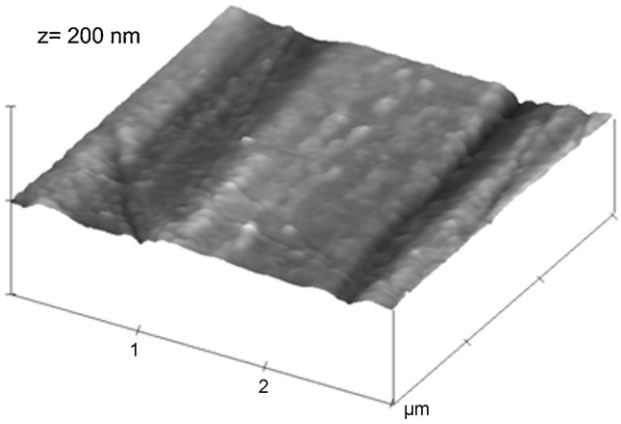

Fig. 1. 3D 3 μm × 3 μm AFM image of polished steel surface.

3. Results and discussion

3.1. Influence of the current pulse program on the surface morphology of the plated Ni–W coatings on carbon steel

AFM observation of the surface features of the substrate was performed after submitting it to the polishing sequence in order to know the initial condition of the surface before the coatings were deposited. Fig. 1 displays the characteristic scratch pattern of polished samples.

Fig. 2 shows 3D AFM images of the deposited coatings on the carbon steel substrate obtained at different τ, but with the same t_{dep} = 60 min. At short τ (10 s) a uniform layer of nanosized grains (≈65 nm) with defined boundaries is observed (Fig. 2(a)). As τ increases, larger grains also appear (ca. 110 nm) in addition to the small ones (ca. 80 nm), presumably associated to the type of growth they experienced (Fig. 2(b)) while grain boundaries remain clearly resolved. Finally, for τ = 120 s, grain size increases to 140 nm and the deposit exhibits a cauliflower-like structure (Fig. 2(c)). These results show that the lower τ is (higher pulse frequency), the smaller the grains obtained are. Also, the τ value allows us to control the film thickness. In fact, when τ changes from 300 s to 5 ms for a constant deposition time t_{dep} = 60 min the film thickness increases from 6 to 15 μm. Thus, the deposit thickness increases with increasing pulse frequency. These findings would indicate that instantaneous current density during τ_{on} is high for a high pulse frequency. This situation will influence the nonsteady state mass transport rate which will affect nucleation velocity and growth mechanisms [23,29].

To analyze how the deposition time (t_{dep}) influences the homogeneity attained in the deposit, the electrodeposition was performed at τ = constant, but at different t_{dep}. The 3D AFM image for τ = 120 s shows that at short t_{dep} (20 min) the characteristic pattern of the carbon steel substrate is still observed (Fig. 3(a)). As t_{dep} increases (60 min), the surface becomes more homogeneous and the characteristic pattern of the substrate disappears (Fig. 3(b)). There are no significant homogeneity changes for t_{dep} over 60 min (Fig. 3(c)) although the electrodeposit becomes thicker.

In the experimental conditions of this work, when the bath pH is decreased to 7.0, keeping a constant pulse program (τ = 120 s and t_{dep} = 120 min), less uniform deposits with more pronounced growth are observed in some places (Fig. 4), in comparison with the obtained coating employing the same pulse program, but at pH 9.5 (Fig. 3(c)). This result is in accordance with those reported by Cesiulis et al. [17] and Younes et al. [18] who determined that there is an optimal pH value for the plating bath where the W–Ni complexes predominate. They would participate in the electroreduction reaction helping to get good quality electrodeposited coatings.

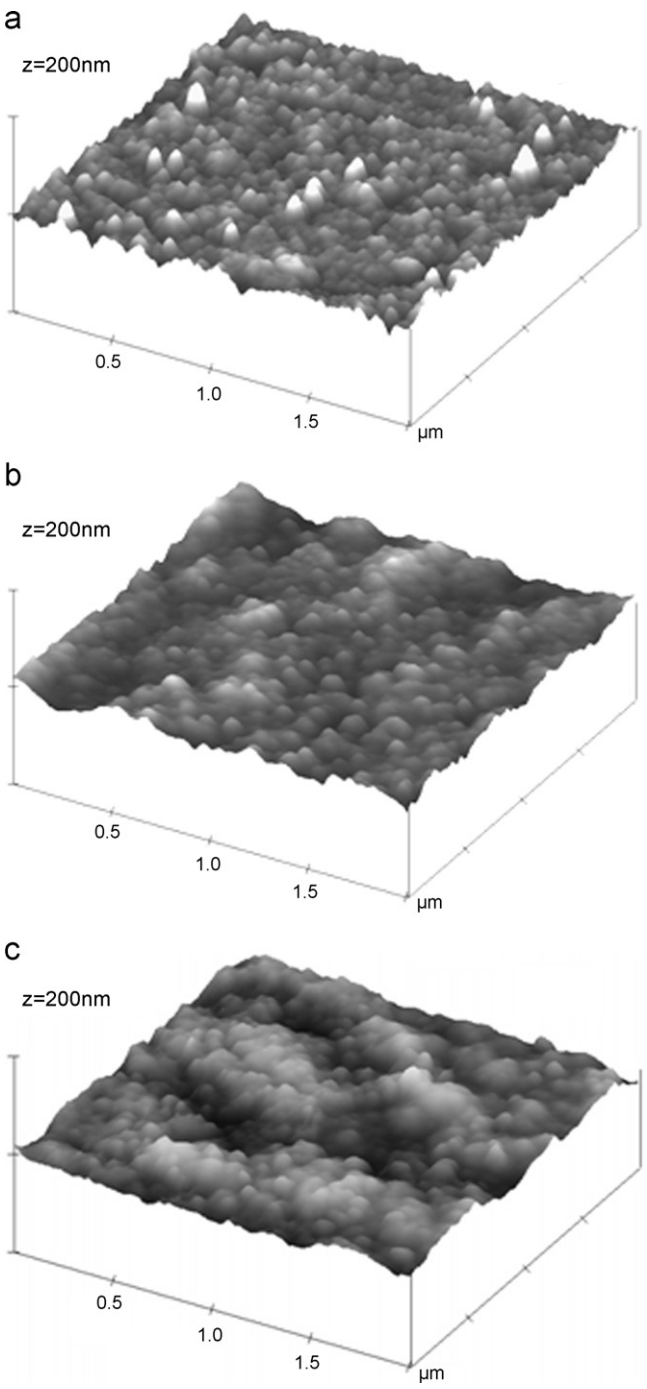

Fig. 2. 3D 2 μm × 2 μm AFM images of Ni–W coatings electrodeposited at the same t_{dep} = 60 min, but different τ: () 10 s, (b) 60 s, (c) 120 s.

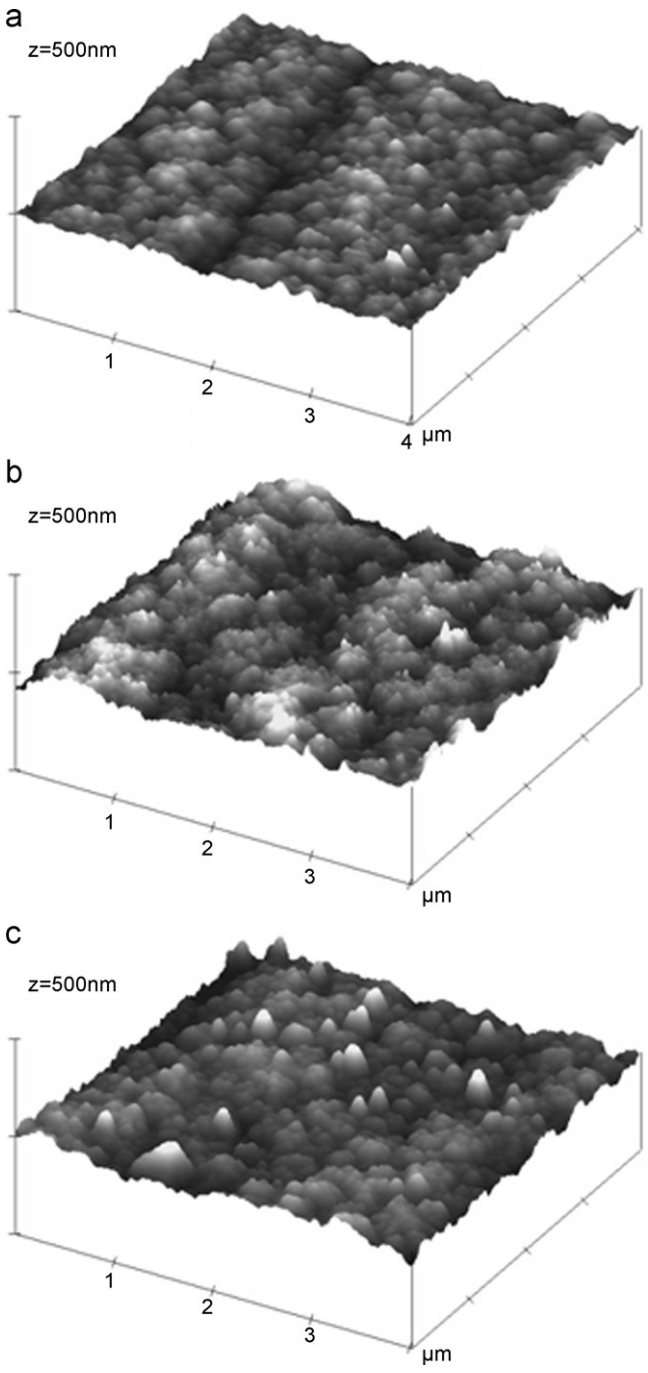

Fig. 3. 3D 4 μm × 4 μm AFM images of Ni–W coatings electrodeposited at the same τ = 120 s, but different t_{dep}: (a) 20 min, (b) 60 min, (c) 120 min.

SEM micrographs for t_{dep} = 60 min clearly show the wide-ranging morphology of the electrodeposit (Fig. 5(a)). A granular distribution (Fig. 5(b)) in the nano-micro scale (already shown in previous AFM data) forms the structure of larger grains with a cauliflower type structure.

3.2. Chemical composition

XPS data of the electrodeposited coatings on the carbon steel substrate show W content in the surface ranging from 15 to 30 at%, depending on the electrodeposition conditions. The most representative data are shown in Table 1.These results indicate that the value

Table 1
XPS data obtained from Ni–W alloy electrodeposited by different current pulse programs.

τ (s)	t_{dep} (min)	Pulse no.	W (at%)
10	60	180	30
120	60	15	29
120	120	30	25
300	120	15	15

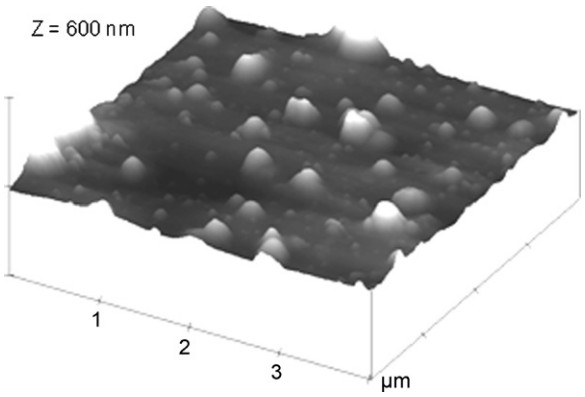

Fig. 4. 3D 4 μm × 4 μm AFM image of Ni–W coatings obtained at pH 7, τ = 120 s and t_{dep} = 120 min.

τ has the most influence in the composition of the surface layer and near-surface layer region, because more W is incorporated in the coating surface for the same cycle number, but with lower τ. The decrease of both the W/Ni concentration ratio and pulse frequency can be assigned to local pH changes that affect the mass transport of Ni species by the formation of a porous Ni hydroxide layer in the alloy surface [18] or to a decrease in the surface concentration of the citrate-tungstate complex [29].

According to XPS measurements, Ni is present in the surface of the electrodeposited coatings in metallic state and in oxides (NiO and NiOOH), and W is present as metal and as oxide (WO_3). After Ar^+ etching WO_3 was found deeper than the Ni oxides, but the WO_3 signal disappears at ≈5 nm from the surface (Fig. 6(a) and (b)). Also, the C signal is a clear evidence that some carbon is present in the bulk of the coating. In fact, a careful analysis of this signal shows that a compound located at 283 eV (Fig. 6(c)) is consistent with the presence of a tungsten carbide and it should certainly contribute to the hardness of the coating. It should be noted that the presence of carbon incorporated in that form has been already reported from citrate containing plating baths [16,35]. On the other hand, the complete absence of Fe in the spectra is consistent with a total coverage of the substrate by the Ni–W layer.

The composition of the different electroplated Ni–W coatings on the carbon steel substrate was also analyzed using EDS. The bulk coating composition was found to be homogeneous as determined by various measurements at different surface locations. The results obtained follow the same tendency as those collected by XPS, although the W content is somewhat lower. Whereas EDS explores ca 1 μm in depth from the surface, in the XPS analysis few nanometers were studied by sputtering. Results obtained from XPS and EDS indicate that the best procedure to obtain the largest W/Ni ratio in the coating is τ = 10 s and t_{dep} = 60 min. In addition, AFM images show the smallest grain size for this condition.

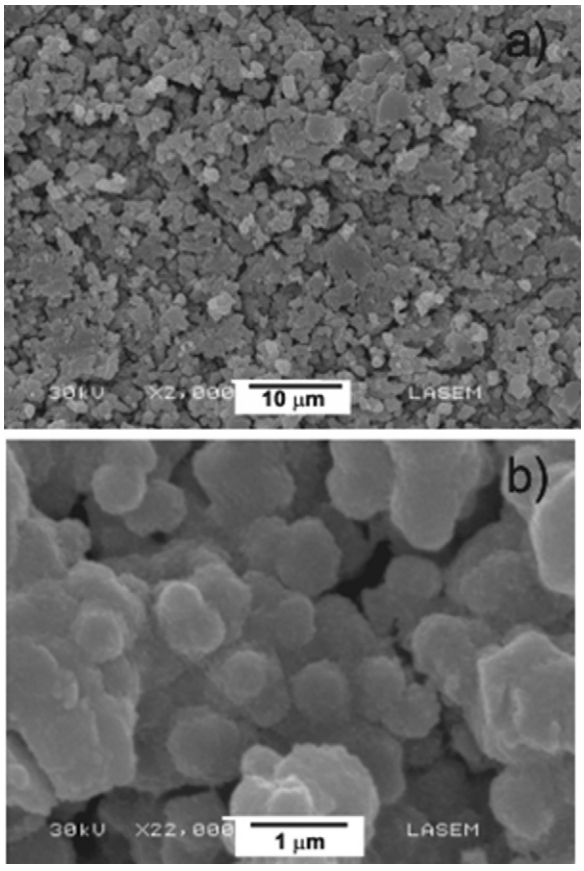

Fig. 5. (a and b) SEM micrographs of the surface of Ni–W coatings deposited at τ = 120 s and t_{dep} = 60 min, for different magnifications.

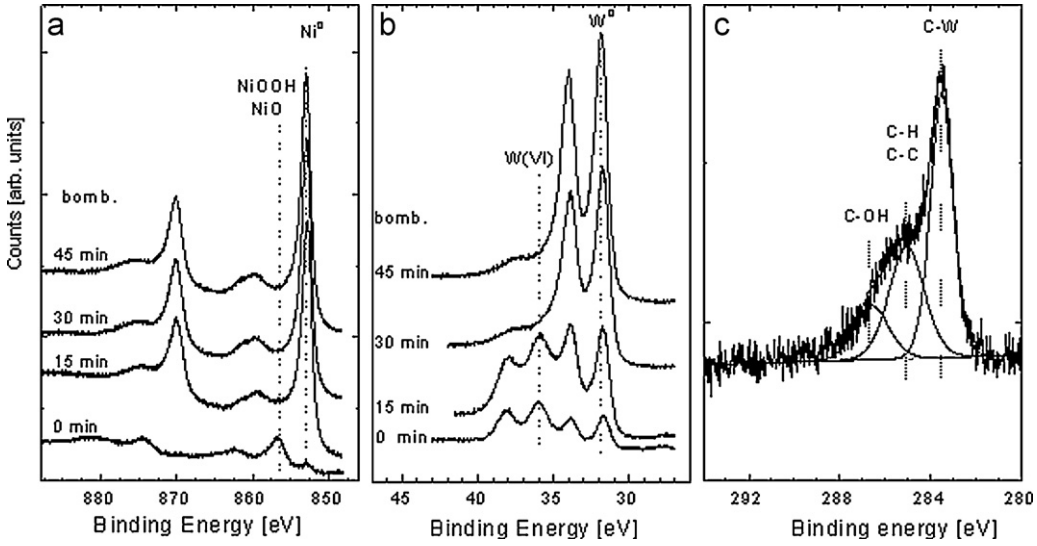

Fig. 6. XPS spectra of a Ni–W coating obtained at τ = 10 s and t_{dep} = 60 min, as plated and after different etching times with Ar^+: (a) Ni 2p region, (b) W 4f region, (c) C 1s region with peak deconvolution.

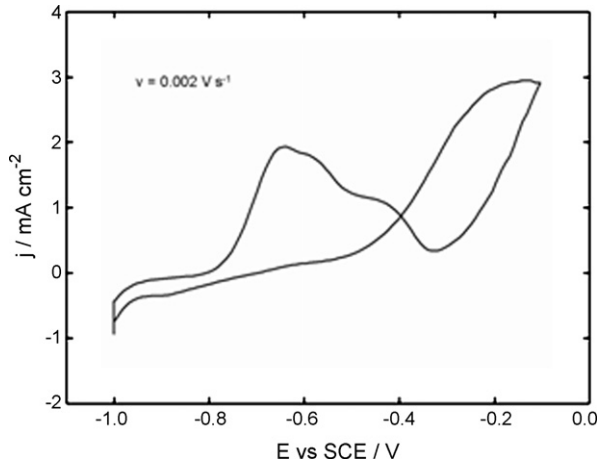

Fig. 7. Carbon steel voltammogram obtained at $\nu = 0.002\,V\,s^{-1}$ in still phosphate-borate buffer solution containing Na_2SO_4 1 M.

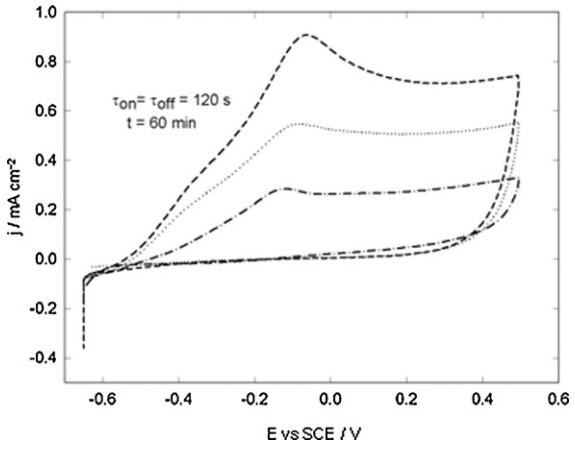

Fig. 8. Ni–W coating voltammograms obtained at different v in still phosphate-borate buffer solution containing Na_2SO_4 1 M: (---) 0.200 Vs^{-1}, (···) 0.100 Vs^{-1}, (--) 0.020 Vs^{-1}.

3.3. Adherence and mechanical properties

The plated Ni–W coatings obtained in the different conditions used in this work show an excellent adhesion to the substrate in contrast to previous results reported by Donten et al. [11] and Yang et al. [24] showing that these coatings adhere poorly to a steel substrate. In fact, the Ni–W coatings produced under the experimental conditions described here were hard to remove from the carbon steel even with the use of mechanical tools. Besides, the surface of the electrodeposits shows the typical Ni–W coating mirror-like shine.

The coatings obtained with the different pulse programs show high microhardness values, between 650 and 850 Hv. This last value corresponds to electrodeposited coatings obtained using $\tau = 10$ s and t_{dep} 60 min. Besides, they do not show signs of brittleness. The lowest hardness value corresponds to $\tau = 120$ s, $t_{dep} = 60$ min, and the corresponding deposits already present certain brittleness. These results agree with the trend, reported in the literature, of increasing hardness and ductility as grain size decreases [15,17,28,30,34].

On the other hand, the low brittleness present in the sample deposited at $\tau = 120$ s, $t_{dep} = 60$ min tends to disappear when deposit thickness increases, probably because residual stress or defects in the bulk coating are lower.

Our results show that deposit grain size and thickness are decisive parameters in the mechanical properties of the Ni–W coating.

3.4. Corrosion behavior of the plated Ni–W carbon steel

Fig. 7 shows a typical voltammogram of the plain carbon steel substrate in still phosphate-borate buffer solution containing 1 M Na_2SO_4 recorded from $E_{s,c} = -1.0$ V to $E_{s,a} = -0.1$ V at $\nu = 0.002\,V\,s^{-1}$. The positive potential exhibits typical anodic current peaks corresponding to the Fe(II) (−0.68 V) and Fe(III) (−0.45 V) hydrous oxides formation [37]. This figure also shows that the anodic current increases suddenly when the potential exceeds −0.38 V due to pit nucleation and growth on the carbon steel surface induced by aggressive sulphate anions. The hysteresis in the voltammogram in the reverse scan corresponds to the growth of the localized corrosion centers that are repassivated at −0.5 V.

A completely different response was observed when the voltammograms were recorded with Ni–W electroplated carbon steel, obtained at $\tau = 120$ s and $t_{dep} = 60$ min (Fig. 8). First, the complete absence of the iron oxide formation is noted. Instead, a well-defined peak located at −0.1 V is observed. This peak, that becomes more defined as the scan rate is increased, corresponds to the NiO formation as reported in [38]. Secondly, the profiles do not exhibit the characteristic hysteresis of pitting corrosion, a fact consistent with the substrate passivation by NiO. It is well known that sulphate anion is unable to promote passivity breakdown and pitting of Ni surfaces.

The voltammogram for the Ni–W coated carbon steel recorded at $\nu = 0.002\,V\,s^{-1}$ (Fig. 9) exhibits current density values one order of magnitude lower than that observed for the plain carbon steel surface (Fig. 7). However, it should be noted that certain anodic current is observed during the reverse scan indicating metal dissolution through the passive film formed on the coating. Besides, the voltammetric response of the Ni–W coatings is not a simple profile superposition of the corresponding metal components. Measurements in the same solution, but using pure Ni and W were also made for the sake of comparison (Fig. 9). The voltammogram corresponding to the Ni electrode indicates that in the potential region between −0.7 V and −0.4 V this metal forms the NiO and remains passive. Besides, the nickel hydroxide layer is not electroreduced in this potential range in the reverse scan. This is in agreement with what was reported by other authors who demonstrated that at the same pH the electrode passivity increases progressively as $E_{s,a}$ becomes more positive [39,40].

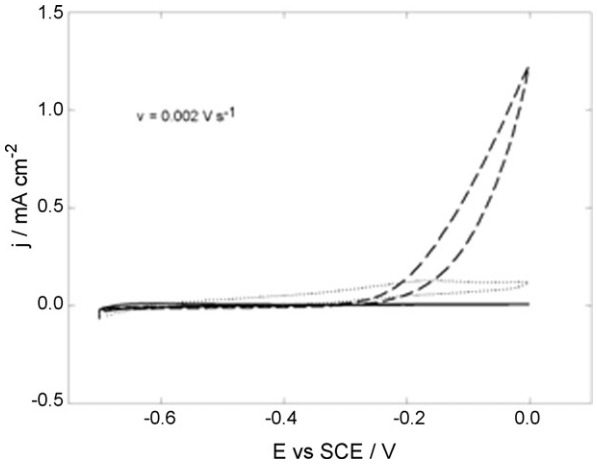

Fig. 9. Voltammograms obtained in still phosphate-borate buffer solution containing Na_2SO_4 1 M of pure Ni (–), pure W (---) and Ni-W (···) coating obtained at $\tau = 120$ s and $t_{dep} = 120$ min.

In contrast to the passive behavior of Ni, tungsten shows dissolution when the potential reaches −0.3 V. The dissolution process should involve oxide formation and dissolution giving tungstate ions [41–43], a fact evidenced by the noticeable current increase shown in Fig. 9. Passivating tungsten oxides are known to be formed at $E_{s,a}$ more positive than 0.2 V, but in these comparative experiments only the pertinent potential region is shown to analyze the carbon steel behaviour.

Thus, the electrodissolution behaviour of the Ni–W coatings, at the pH value used in this work, is defined by the W contribution based on what was previously analyzed. Surface W and WO_3 (detected by XPS) tend to dissolve during the anodic potential sweep with the corresponding Ni enrichment at the interface. On the other hand, the protecting properties observed at anodic potentials were mainly due to the passivating Ni oxides (Fig. 9). Additionally, such anodic current diminution is enhanced with a longer t_{dep}, for which a thicker deposit is obtained, according to results described in Section 3.1 and data included in Table 1. Structural and morphological changes in the film should not be discarded [16]. These results evidence that corrosion behavior is sensitive to structural characteristics, and therefore it will depend on the preset electrodeposition conditions [33].

4. Conclusions

(1) Hard, ductile and adherent nanostructured Ni–W coatings were electrodeposited on carbon steel from an electrolyte solution of pH 9.5 containing sodium tungstate, nickel sulphate and sodium citrate, using different current pulse programs.
(2) Current pulse frequency was the dominant factor to define chemical composition, grain size, thickness, hardness and corrosion resistance of the Ni–W coating. The deposited coating incorporated between 15 and 30 at% W, grain size ranged from 65 to 140 nm, hardness varied from 650 to 850 Hv, and steel substrate adhesion was excellent. Tungsten carbide present in the coating contributed to its high hardness.
(3) The Ni–W coating provided good corrosion resistance to the carbon steel in sulphate containing electrolytes. While some dissolution of W took place, nickel oxides provided a protective barrier that inhibited localized corrosion.

Acknowledgements

The authors acknowledge financial support from the Consejo Nacional de Investigaciones Científicas y Técnicas (CONICET, PIP0362), the Agencia Nacional para la Promoción de la Ciencia y la Tecnología (ANPCyT, PAE 22711), Argentina, and the Consejo de Investigaciones de la Universidad Nacional de Tucumán, Argentina. M.E.Vela is a member of the research career of CIC BsAs.

The authors wish to thank Ing. Carlos Llorente (LIMF, Facultad de Ingeniería, Universidad Nacional de La Plata, Argentina) for carrying out hardness determinations.

References

[1] A. Brenner, Electrodeposition of Alloys vol. II, Academic Press, New York, 1963.
[2] A.R. Despić, V.D. Jović, R.E. White, J.O.M. Bockris, in: B.E. Conway (Ed.), Modern Aspects of Electrochemistry, no. 27, Plenum Press, New York, 1995 (Chapter 2).
[3] C.C. Nee, W. Kim, R. Weil, J. Electrochem. Soc. 135 (1988) 1100.
[4] M. Donten, Z. Stojek, J. Appl. Electrochem. 26 (1996) 665.
[5] S. Yao, S. Zhao, H. Guo, M. Kowaka, Corrosion 52 (1996) 183.
[6] E.J. Podlaha, D. Landolt, J. Electrochem. Soc. 143 (1996) 885.
[7] M. Bratoeva, N. Atanassov, Met. Finish. 96 (1998) 92.
[8] T. Yamasaki, P. Schloβmacher, K. Ehrlich, Y. Ogino, NanoStruct. Mater. 10 (1998) 375.
[9] L.I. Stepanova, O.G. Purovskaya, Met. Finish. 96 (1998) 50.
[10] T. Yamasaki, Mater. Phys. Mech. 1 (2000) 127.
[11] M. Donten, H. Cesiulis, Z. Stojek, Electrochim. Acta 45 (2000) 3389.
[12] P. Schloβmacher, T. Yamasaki, Mikrochim. Acta 132 (2000) 309.
[13] M.D. Obradović, J. Stevanović, R.M. Stevanović, A.R. Despić, J. Electroanal. Chem. 491 (2000) 188.
[14] O. Younes, E. Gileadi, Electrochem. Solid-State Lett. 3 (2000) 543.
[15] O. Younes, L. Zhu, Y. Rosenberg, Y. Shacham-Diamond, E. Gileadi, Langmuir 17 (2001) 8270.
[16] M. Obradović, J. Stevanović, A. Despić, R. Stevanović, J. Stoch, J. Serb. Chem. Soc. 66 (2001) 899.
[17] H. Cesiulis, A. Baltutiene, M. Donten, M.L. Donten, Z. Stojek, J. Solid State Electrochem. 6 (2002) 237.
[18] O. Younes, E. Gileadi, J. Electrochem. Soc. 149 (2002) C100.
[19] L. Zhu, O. Younes, N. Ashkenasy, Y. Shacham-Diamond, E. Gileadi, Appl. Surf. Sci. 200 (2002) 1.
[20] A. Marlot, P. Kern, D. Landolt, Electrochim. Acta 48 (2002) 29.
[21] M. Donten, Z. Stojek, H. Cesiulis, J. Electrochem. Soc. 150 (2003) C95.
[22] O. Younes-Metzler, L. Zhu, E. Gileadi, Electrochim. Acta 48 (2003) 2551.
[23] D. Landolt, A. Marlot, Surf. Coat. Technol. 169 (2003) 8.
[24] F.-Z. Yang, Y.-F. Guo, L. Huang, S.-K. Xu, S.-M. Zhou, Chin. J. Chem. 22 (2004) 228.
[25] M. Donten, H. Cesiulis, Z. Stojek, Electrochim. Acta 50 (2005) 1405.
[26] T.M. Sridhar, N. Eliaz, E. Gileadi, Electrochem. Solid-State Lett. 8 (2005) C58.
[27] N. Eliaz, T.M. Sridhar, E. Gileadi, Electrochim. Acta 50 (2005) 2893.
[28] K.R. Sriraman, S. Ganesh Sundara Raman, S.K. Seshadri, Mater. Sci. Eng. A 418 (2006) 303.
[29] M.D. Obradović, G.Ž. Bošnjakov, R.M. Stevanović, M.D. Maksimović, A.R. Despić, Surf. Coat. Technol. 200 (2006) 4201.
[30] A.J. Detor, C.A. Schuh, Acta Mater. 55 (2007) 371.
[31] K.R. Sriraman, S. Ganesh Sundara Raman, S.K. Seshadri, Mater. Sci. Eng. A 460 (2007) 39.
[32] Y. Xuetao, W. Yu, S. Dongbai, Y. Hongying, Surf. Coat. Technol. 202 (2008) 1895.
[33] A. Krolikowski, E. Plonska, A. Ostrowski, M. Donten, Z. Stojek, J. Solid State Electrochem. 13 (2009) 263.
[34] M.F. Cardinal, P.A. Castro, J. Baxi, H. Liang, F.J. Williams, Surf. Coat. Technol. 204 (2009) 85.
[35] R. Juškėnas, I. Valsiūnas, V. Pakštas, R. Giraitis, Electrochim. Acta 54 (2009) 2616.
[36] A.M. El-Sherik, U. Erb, J. Page, Surf. Coat. Technol. 88 (1996) 70.
[37] C.C. Acosta, R.C. Salvarezza, H.A. Videla, A.J. Arvia, Corros. Sci. 25 (1985) 291.
[38] D.V. Vásquez Moll, R.C. Salvarezza, H.A. Videla, A.J. Arvia, J. Electrochem. Soc. 132 (1985) 754.
[39] L.M. Gassa, J.R. Vilche, A.J. Arvia, J. Appl. Electrochem. 13 (1983) 135.
[40] G. Barral, F. Njanjo-Eyoke, S. Maximovitch, Electrochim. Acta 28 (2005) 709.
[41] P.I. Ortiz, M. López Teijelo, M.C. Giordano, J. Electroanal. Chem. 243 (1988) 379.
[42] M. Anik, K. Osseo-Asare, J. Electrochem. Soc. 149 (2002) B224.
[43] M. Anik, Corros. Sci. 52 (2010) 3109.